*Revised manuscript (om-2014-01292k)*

# Coordination Induced Atropisomerism in a NHC-based Rhodium Macrocycle

Rhiann E. Andrew,[a] Dominic W. Ferdani,[a] C. André Ohlin[b] and Adrian B. Chaplin*[a]

[a] *Department of Chemistry, University of Warwick, Gibbet Hill Road, Coventry CV4 7AL, UK.*

E-mail: a.b.chaplin@warwick.ac.uk

[b] *School of Chemistry, Monash University Clayton, Victoria 3800, Australia.*

**Abstract**

Reversible interaction with carbon monoxide results in the onset of dynamic atropisomerism at 298 K in an otherwise static NHC-based rhodium pincer complex, [Rh(C^N^C-$(CH_2)_{12}$)(CO)][$BAr^F_4$] (**1**, $Ar^F$ = 3,5-$C_6H_3(CF_3)_2$). The mechanism of this process has been comprehensively interrogated by a combination of variable temperature NMR spectroscopy, IR spectroscopy, and computational modeling. In addition, a structural analogue of a high-energy symmetrical intermediate species – invoked in the process but not directly observed spectroscopically – has been prepared and characterised in solution and the solid-state.

**TOC graphic**

## Introduction

Pincer ligand architectures featuring *N*-heterocyclic carbene (NHC) donors are becoming increasingly prominent in organometallic chemistry, combining the strong σ-donor characteristics of NHCs with the favourable thermal stability and reaction control possible with a mer-tridentate geometry.[1,2] In particular, CCC and CNC ligands featuring *trans*-NHC donors have been partnered with a wide variety of transition elements and subsequently exploited in numerous catalytic transformations.[3,4] The structures of xylene- and lutidine-based CCC and CNC variants exhibit characteristically twisted $C_2$ geometries, which orientate the NHC wingtips (R in Scheme 1) onto opposite faces of the coordination plane. Interconversion between the chiral conformations, atropisomerism, can result in structural fluxionality, even at ambient temperature, and has important consequences for the steric profile of the ligand.[5,6,7] Notably, such dynamics are undesirable in any potential applications of CCC and CNC ligands in asymmetric catalysis.[8]

**Scheme 1:** Atropisomerism in xylene- (E = $C^-$) and lutidine-based (E = N) NHC pincer complexes

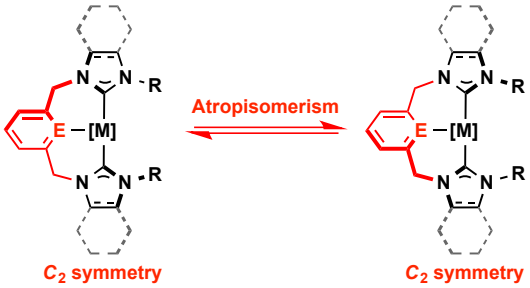


**Chart 1**

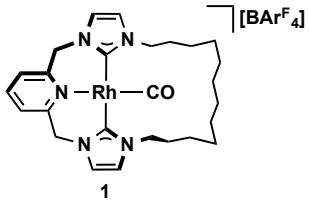


**1**

Previously, the atropisomerism of NHC-based pincer systems has almost exclusively been investigated using Pd(II) complexes, with lutidine-based pincer complexes characterised by *ca* 20 kJ·mol$^{-1}$ lower barriers than comparable xylene variants.[5,6] Broadly speaking little barrier height variation is found between systems containing *n*-alkyl wingtips or macrocyclic variants with flexible methylene-based linkers;[5,6,9] bulky aryl appendages appear to attenuate atropisomerism.[10] Mechanistic work by Faller, Eisenstein and Crabtree has firmly established mechanisms involving $C_s$ symmetric intermediates, with the more facile atropisomerism of Pd(II) CNC complexes suggested to proceed via pathways involving partial or complete lutidine dissociation.[5] This suggestion was upheld computationally and by experimental observations that implicated coordination of the counter anion during the process. With a view to exploiting their unique steric profile and topology in organometallic and supramolecular chemistry, some of us have recently become engaged in the investigation of macrocyclic CNC-based complexes such as rhodium(I) complex **1** (Chart 1, $Ar^F$ = 3,5-$C_6H_3(CF_3)_2$).[9,11] In this report, we describe atropisomerism of **1** that is unusually induced on addition of carbon monoxide and comprehensively interrogate the mechanism of this process.

**Results and discussion**

Complex **1** adopts $C_2$ symmetry in $CD_2Cl_2$ solution across a wide temperature range (185 – 308 K).[11] The high symmetry purports conformational rigidity of the lutidine-based CNC backbone and facile accommodation of the carbonyl ancillary ligand within the macrocycle cavity. To ascertain the barrier for atropisomerism, **1** was studied at higher temperatures by variable temperature $^1$H NMR spectroscopy using $C_6D_6$ as a solvent (298 – 350 K, 500 MHz). Coalescence of the diastereotopic methylene bridge (py$CH_2$) and *N*-methylene (*N*-$CH_2CH_2$) resonances is apparent at 350 K and an activation barrier of $\Delta G^{\ddagger}$(298 K) = +66 ± 8 kJ·mol$^{-1}$ was obtained by simulation of the $^1$H NMR data and an Eyring analysis (Figures S9 and S10; $\Delta H^{\ddagger}$ = +62 ± 4 kJ·mol$^{-1}$, $\Delta S^{\ddagger}$ = -15 ± 13 J·mol$^{-1}$·K$^{-1}$). Placing a solution of **1** in $CD_2Cl_2$ (11 mM) inside a J. Young's NMR tube under 1 atmosphere of carbon monoxide[12] results in the observation of time-averaged $C_{2v}$ symmetry in the $^1$H NMR spectrum indicating a reversible reaction between **1** and CO that involves atropisomerism (400 MHz, Figure 1). Removing carbon monoxide by successive freeze-pump-thaw (FPT) cycles gradually halts the dynamics and regenerates **1**, but only after *ca* 18 cycles. To further investigate this fluxional process, we again turned to variable temperature $^1$H NMR spectroscopy (1 atm CO, $CD_2Cl_2$, 500 MHz; Figure 1). Cooling to 185 K resulted in (partial) decoalescence and a barrier height of $\Delta G^{\ddagger}$(298 K) = +40 ± 9 kJ·mol$^{-1}$ was determined from the data by line shape analysis as function of temperature and ascribed to atropisomerism of the pincer backbone (Figure S11 and S12; $\Delta H^{\ddagger}$ = +38 ± 4 kJ·mol$^{-1}$, $\Delta S^{\ddagger}$ = -9 ± 17 J·mol$^{-1}$·K$^{-1}$). At 185 K the signals observed do not correspond directly to **1** and are consistent with the presence of/dynamic exchange with a new $C_2$ or $C_s$ symmetric species: the chemical shifts of the diastereotopic methylene bridge resonances (δ 5.21/4.80; $^2J_{HH}$ = 14.2 Hz) are notably disparate from those observed for **1** at 185 K (δ 5.31/5.03; $^2J_{HH}$ = 15.0 Hz).[11]

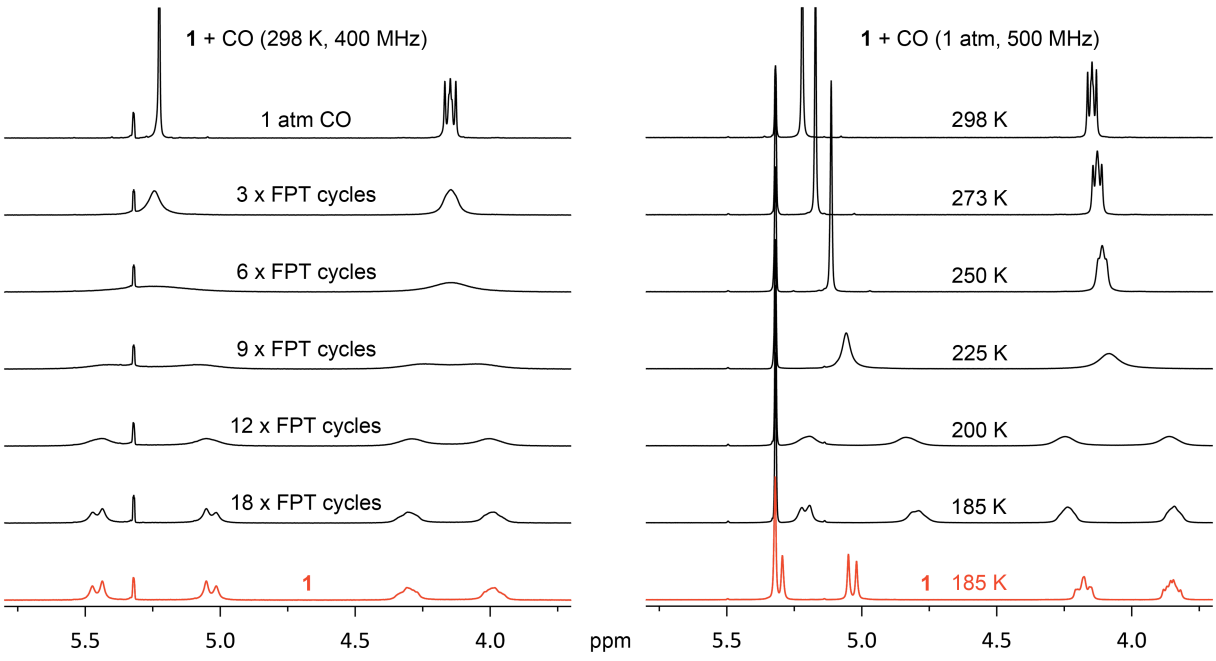


**Figure 1**: $^1$H NMR spectra of interaction of **1** (11 mM) with CO in $CD_2Cl_2$ solution recorded under different CO regimes (left) and temperatures (right). Spectra of **1** shown in red for comparison (lower traces).

On the basis of previous work on related palladium compounds (*vide supra*) and using a more amenable *N*-methyl analogue (**1'**),[13] two alternative fluxional mechanisms have been computationally evaluated for the dynamics of **1**: a one-step process involving $C_2$ symmetric intermediate **2'** and a two-step process, where twisting of the pincer ligand is preceded by coordination of carbon monoxide (Scheme 2). All calculations were carried out using density functional theory (DFT) using the dispersion-inclusive exchange correlation functional M06,[14] and combinations of the Stuttgart RSC 1997 ECP (Rh) and 6-31G(d,p) (C,H,N,O) basis sets.[15,16] Pathways invoking dissociation of CO and formation of low-coordinate **3'** are unlikely under the experimental conditions and associated with a prohibitively large calculated reaction enthalpy (+240 kJ·mol$^{-1}$) and associated free energy (+198 kJ·mol$^{-1}$).

**Scheme 2**: Mechanic schemes associated with the atropisomerism of **1'**. Calculated free energies in kJ·mol$^{-1}$ at 298 K.

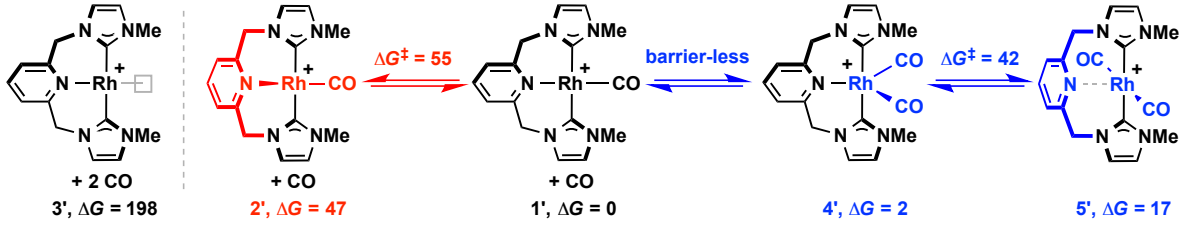


Using the Nudged Elastic Band (NEB) method[17] the overall barrier for the one step atropisomerism mechanism via twisting of the $\kappa^3$-coordinated pincer ligand (**1'**⇌**2'**) was calculated to be $\Delta H^{\ddagger}$(298 K) +53 / $\Delta G^{\ddagger}$(298 K) +55 kJ·mol$^{-1}$, consistent with the relatively high value observed experimentally for **1** in the absence of CO ($\Delta G^{\ddagger}$(298 K) = +66 ± 8 kJ·mol$^{-1}$). The lutidine remains tightly coordinated throughout the process; the transition state is characterised by a Rh–N bond length of 2.24 Å, only marginally longer than for **1'** (2.19 Å) and very similar to **2'** (2.25 Å) – the associated calculated (NAO) bond order changes by less than 5% (Table S2). The alternative mechanism proceeds with a significantly exothermic, but marginally endergonic addition of CO to **1**' to form intermediate **4'** ($\Delta H$(298 K) -41 /$\Delta G$(298 K) +2 kJ·mol$^{-1}$). The calculated NEB trajectory for this process showed only a smooth increase in energy, inferring a barrier-less process. The coordination of a second CO ligand results in significant elongation of the Rh–N bond (2.41 Å) and corresponding reduction in NAO bond order (by 18%). Such characteristics enable a much lower barrier for atropisomerism (**4'**⇌**5'**; $\Delta H^{\ddagger}$(298 K) +46 / $\Delta G^{\ddagger}$(298 K) +42 kJ·mol$^{-1}$), with $C_s$ symmetric intermediate **5'** featuring an essentially $\kappa^2$-coordinated pincer ligand (Rh···N = 2.63 Å; 54% lower Rh···N NAO bond order than **1'**). These characteristics are in excellent agreement with the variable temperature $^1$H NMR data; in particular the measured barrier for atropisomerism: $\Delta G^{\ddagger}$(298 K) = +40 ± 9 kJ·mol$^{-1}$. In view of the calculated thermodynamics, the 185 K NMR spectrum of **1** under CO is interpreted as being the result of rapid equilibration between **1** and a 5-coordinate bis-carbonyl adduct **4** on the relatively slow time frame of the experiment. It is this latter species in solution that presumably helps counteract removal of CO in solution, necessitating numerous freeze-pump-thaw cycles.

To further experimentally probe the apparent dynamics observed by $^{1}$H NMR at 185 K, the interaction of **1** with CO was studied by *in situ* IR spectroscopy using a sealed solution cell (1 atm CO, $CH_2Cl_2$, 298 K). In addition to the ν(CO) band associated with **1** (1978 $cm^{-1}$), carbonyl signals are observed at 2007 and 1953 $cm^{-1}$ in the difference spectrum which we attribute to **4** (aided by comparison to the spectrum of **6**, *vide infra*); the two compounds are now in slow exchange relative to the *rapid* IR time scale (Figure 2).[18] The IR spectrum is, however, heavily dominated by the carbonyl stretching of **1**, experimentally establishing it as the ground state configuration under CO at 298 K. The relative intensity of the bands attributed to **4**, and the presence of only two species provides strong corroboration of the calculated trends in free energies described above for the intermediates involved in the atropisomerism of **1'**.

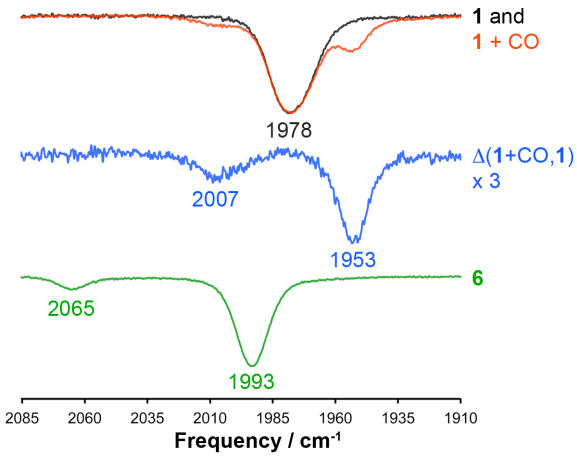


**Figure 2**: IR spectra of **1** (black), **1** + CO (1 atm, red) and **6** (green) recorded in $CH_2Cl_2$ (298 K, transmission mode). Difference spectrum (**1** + CO, **1**) in blue was taken using normalized transmissions at 1978 $cm^{-1}$.

In parallel to the computational and spectroscopic studies, rhodium(I) bis-carbonyl **6** was prepared as a structural analogue of the calculated intermediate **5'**. Complex **6** was obtained from a readily accessible bis(imidazolium)-xylene pro-ligand using our previously described $Ag_2O$-based transmetallation strategy in combination with $[Rh(CO)_2Cl]_2$ and $Na[BAr^F_4]$, and ultimately isolated in 46% yield following purification by column chromatography (Scheme 3). Alongside the solid-state structure determined by X-Ray diffraction, the structure of **6** was fully corroborated by NMR and IR spectroscopy, together with ESI-MS and elemental analysis (Figure 3). The relative frequencies of the ν(CO) bands add experimental support to the attribution of the additional bands observed when **1** is placed under CO, i.e. to 5-coordinate bis-carbonyl adduct **4** rather than 4-coordinate bis-carbonyl adduct **5**. The solid-state structure of **6** is particularly notable for the distinctly bent *trans*-carbonyl ligands (OC-Rh-CO = 151.8(2)º) and the tilted aryl group, which is held in close proximity to the metal centre (Rh1···C1 = 2.585(5) Å). Although similar distorted saw-horse geometries have been reported for $d^8$-metal bis-carbonyl compounds, *e.g.* *trans*-$[Ir(PPh_3)_2(CO)_2]^+$ (OC-Ir-CO = 165.9(2)º),[19] the only structurally characterised NHC precedent to our knowledge, *trans*-$[Rh(IBioxMe_4)_2(CO)_2]^+$, features an essentially linear configuration (OC-Rh-CO = 173.46(11)º; ν(CO) = 2024 $cm^{-1}$).[20] The measured $^{1}J_{CH}$ coupling constant for the aryl C–H bond is unchanged in comparison to the free ligand (158 Hz; cf. 159 Hz)

suggesting that no agostic interaction is present despite the proximity of the bond to the metal centre.[21] Instead, we suggest the presence of a weak C($p_\pi$)-based interaction; consistent with this suggestion there is a non negligible Rh···C NAO bond order in the computed *N*-methyl analogue **6'**, which is of very similar magnitude to that calculated for the Rh···N interaction in **5'** (see Table S2) – helping validate the use of **6** as a model for **5**.

**Scheme 3**: Preparation of model intermediate **6**.[a]

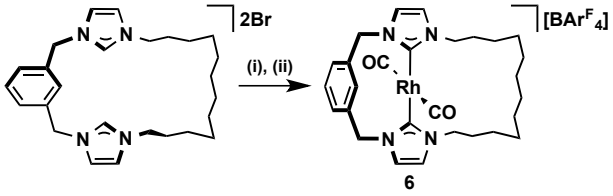


[a] Reagents and conditions: (i) $Ag_2O$ and $Na[BAr^F_4]$, $CH_2Cl_2$, RT; (ii) $[Rh(CO)_2Cl]_2$, $CH_2Cl_2$, RT.

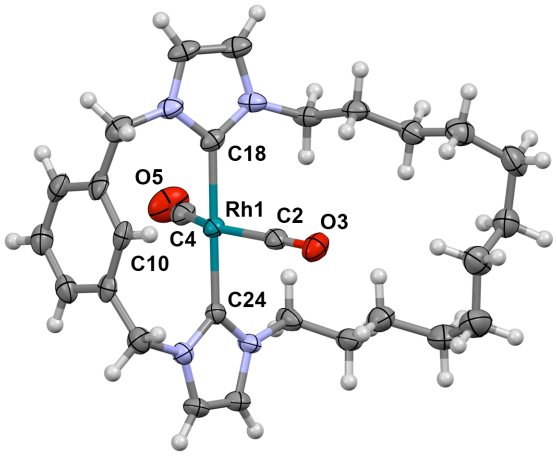


**Figure 3**: Solid-state structure of **6**. Thermal ellipsoids drawn at the 50% probability levels; anion and solvent molecule omitted for clarity. Selected bond lengths (Å) and angles(º): Rh1-C2, 1.895(6); Rh1-C4, 1.914(6); Rh1···C10, 2.585(5); Rh1-C18, 2.067(5); Rh1-C24; 2.050(5); C2-Rh1-C4, 151.8(2); C18-Rh1-C24, 178.8(2).

**Summary**

Insights into the structural dynamics of $C_2$ symmetric NHC based-pincer complexes have been gained through a combined computational and experimental investigation of a macrocyclic CNC-based rhodium(I) complex (**1**). In isolation, atropisomerism of **1** is encumbered by coordination of the central lutidine moiety to the metal centre throughout the process ($\Delta G^{\ddagger}$(298 K) = +66 ± 8 kJ·mol$^{-1}$). Under a CO atmosphere structural fluxionally is induced, with reversible coordination of CO promoting a more facile atropisomerism mechanism involving dissociation of the lutidine moiety, twisting of the pincer backbone, and re-coordination of the lutidine bridge ($\Delta G^{\ddagger}$(298 K) = +40 ± 9 kJ·mol$^{-1}$) – giving an overall barrier for the atropisomerism of **1** of approximately $\Delta G^{\ddagger}$(298 K) = +42 kJ·mol$^{-1}$. The presence of a low-energy bis-carbonyl intermediate (**4**) has been directly verified by in situ IR spectroscopy and a structural analogue (**6**) of a second (high energy) $C_2$ symmetric intermediate species (**5**) has been prepared to help substantiate the proposed two-step atropisomerism mechanism under CO.

## Experimental

### General experimental methods

Manipulations were performed under an inert atmosphere, using Schlenk (nitrogen) and glove box (argon) techniques unless otherwise stated. Glassware was oven dried (150ºC) and flamed under vacuum prior to use. Anhydrous solvents (<0.005% $H_2O$) were purchased from ACROS or Aldrich and used as supplied: $CH_2Cl_2$, $CHCl_3$, 1,4-dioxane and MeCN. $CD_2Cl_2$ was dried over $CaH_2$, vacuum distilled, and stored under argon. $C_6D_6$ was dried over sodium, vacuum distilled, and stored under argon. $Na[BAr^F{}_4]$,[22] $[Rh(CO)_2Cl]_2$,[23] 1,12-bis(imidazole)dodecane[9] and **1**[11] were synthesised using literature procedures. All other reagents are commercial products and were used as received. NMR spectra were recorded on Bruker DPX-400, AV-400, AV-500 (variable temperature experiments) and AVIII-500 HD spectrometers at 298 K unless otherwise stated. Chemical shirts are quoted in ppm; coupling constants are given in Hz. IR spectra were recorded in $CH_2Cl_2$ (1.2 mM) using a cell with a Perkin Elmer spectrum100 spectrometer. ESI-MS were recorded on a Bruker MaXis mass spectrometer. Microanalyses were performed at the London Metropolitan University by Stephen Boyer.

### Synthesis of new compounds

$[C\text{^}CH\text{^}C\text{-}(CH_2)_{12}](Br)_2$

Solutions of α,α'-Dibromo-m-xylene (1.00 g, 3.79 mmol) and 1,12-bis(imidazole)dodecane (1.25 g, 3.79 mmol) in 1,4-dioxane (*ca* 0.075 M) were simultaneously added dropwise over 30 minutes to a flask charged with warm 1,4-dioxane (150 mL, 90°C). The suspension was heated at reflux for 16 hours, cooled, and the solvent removed in vacuo. The resulting off-white residue was extracted with MeCN (*ca* 200 mL) with vigorous stirring. The MeCN solution was filtered, concentrated and excess $Et_2O$ added. The resulting precipitate was isolated by filtration and washed with excess $Et_2O$ to obtain the product as a white crystalline solid. Yield: 0.50 g (23%). **$^1$H NMR** (500 MHz, $CD_2Cl_2$): δ 10.66 (app. t, *J* = 1, 2H, imid), 8.23 (app. t, *J* = 2, 2H, imid), 8.10 (app. t, *J* = 2 Hz, 1H, aryl), 7.62 (dd, $^3J_{HH}$ = 7.7, *J* = 2, 2H, aryl), 7.34 (t, $^3J_{HH}$ = 7.6, 1H, aryl), 7.32 (app. t, *J* = 2, 2H, imid), 5.63 (s, 4H, (aryl)C$\underline{H}_2$), 4.27 (t, $^3J_{HH}$ = 7.2, 4H, *N*-$CH_2$), 1.90 (app. p, *J* = 7, 4H, $CH_2$), 1.18 – 1.32 (m, 16H, $CH_2$). **$^{13}$C{$^1$H} NMR** (126 MHz, $CD_2Cl_2$): δ 137.8, 135.4, 131.5, 130.4, 130.4, 123.9, 122.0, 54.0, 53.0, 50. 5, 29.7, 28.6, 28.3, 28.2, 25.8. **$^{13}$C NMR** (126 MHz, $CD_2Cl_2$, selected signal only): δ 131.5 (d app. p, $^1J_{CH}$ = 159, *J* = 4, aryl C10). **ESI-MS** ($CH_3CN$, 180 °C, 3 kV) positive ion: 203.155 *m/z* $[M]^{2+}$ (calc. 203.154). **Anal.** Calcd. for $C_{26}H_{38}Br_2N_4$ (566.144 $gmol^{-1}$): C, 55.13; H, 6.76; N, 9.89. Found: C, 55.20; H, 6.90; N, 9.80.

$[Rh(C\text{^}CH\text{^}C\text{-}(CH_2)_{12})(CO)_2][BAr^F{}_4]$ (**6**)

To a Schlenk flask charged with $[C\text{^}CH\text{^}C\text{-}(CH_2)_{12}](Br)_2$ (0.140 g, 0.247 mmol), $Ag_2O$ (0.057g, 0.247 mmol) and $Na[BAr^F{}_4]$ (0.239g, 0.269 mmol) was added $CH_2Cl_2$ (5 mL). The resulting solution was stirred at room temperature for 16 hours, a solution of $[Rh(CO)_2Cl]_2$ (0.048, 0.124mmol) in $CH_2Cl_2$ (2 mL) added, and then stirred for a further 53 hours. The solution was then filtered and passed through a silica plug ($CH_2Cl_2$). The

product was precipitated as a yellow solid by addition of excess pentane. Yield = 0.162 g (46%). **$^{1}$H NMR** (500 MHz, $CD_2Cl_2$): δ 8.52 (s, 1H, aryl C10H), 7.70 – 7.75 (m, 8H, $Ar^F$), 7.56 (s, 4H, $Ar^F$), 7.52 (t, $^{3}J_{HH}$ = 7.7, 1H, aryl), 7.36 (dd, $^{3}J_{HH}$ = 7.6, *J* = 2, 2H, aryl), 7.20 (d, $^{3}J_{HH}$ = 2.0, 2H, imid), 7.12 (d, $^{3}J_{HH}$ = 2.1, 2H, imid), 5.09 (d, $^{2}J_{HH}$ = 13.0, 2H, (aryl)C$\underline{H}_2$), 5.02 (d, $^{2}J_{HH}$ = 13.0, 2H, (aryl)C$\underline{H}_2$), 4.19 (t, $^{3}J_{HH}$ = 8.2, 4H, *N*-$CH_2$), 1.66 – 1.81 (m, 4H), 1.25 – 1.42 (m, 16H). **$^{13}$C{$^{1}$H} NMR** (126 MHz, $CD_2Cl_2$): δ 187.8 (d, $^{1}J_{RhC}$ = 74, carbonyl), 182.4 (d, $^{1}J_{RhC}$ = 69, carbonyl), 167.7 (d, $^{1}J_{RhC}$ = 37, carbene), 162.3 (q, $^{1}J_{CB}$ = 49, $Ar^F$), 139.5 (s, aryl), 135.4 (s, $Ar^F$), 130.8 (s, aryl), 129.4 (qq, $^{2}J_{FC}$ = 32, $^{3}J_{BC}$ = 3, $Ar^F$), 129.4 (s, aryl), 125.1 (q, $^{1}J_{FC}$ = 272, $Ar^F$), 124.8 (s, imid), 122.0 (s, imid), 118.1 (sept, $^{3}J_{FC}$ = 4, $Ar^F$), 110.8 (s, aryl C10), 54.8 (s, (aryl)C$\underline{H}_2$), 54.4 (s, *N*-$CH_2$), 31.2 (s, $CH_2$), 27.3 (s, $CH_2$), 27.2 (s, $CH_2$), 25.8 (s, $CH_2$), 25.6 (s, $CH_2$). **$^{13}$C NMR** (126 MHz, $CD_2Cl_2$, selected signal only): δ 110.8 (d app. p, $^{1}J_{CH}$ = 157, *J* = 4, aryl C10). **ESI-MS** ($CH_3CN$, 180 °C, 3 kV) positive ion: 563.189 *m*/*z*, $[M]^+$ (calc. 563.188). **Anal.** Calcd. for $C_{60}H_{48}BF_{24}N_4O_2Rh$ (1426.75 $gmol^{-1}$): C, 50.51; H, 3.39; N, 3.93. Found: C, 50.35; H, 3.24; N, 4.14. **IR** ($CH_2Cl_2$): *ν*(CO) 1993 $cm^{-1}$ (s), 2065 $cm^{-1}$ (w). Full crystallographic details for **6** are documented in CIF format and have been deposited with the Cambridge Crystallographic Data Centre under CCDC 1038863. These data can be obtained free of charge from The Cambridge Crystallographic Data Centre via www.ccdc.cam.ac.uk/data_request/cif.

**Computational details**

Geometry optimizations, normal mode analyses and nudged elastic band (NEB) reaction modeling were all performed using NWChem 6.5; NEB was carried out using a step size and spring constant of 1.0.[17,24] Natural Bond Order analyses were carried out using Gaussian 09.[25] All calculations were carried out using the M06 exchange correlation functional,[14] using the Stuttgart RSC 1997 ECP (Rh) and 6-31G(d,p) (C,H,N,O) basis sets.[15] Initial NEB trajectories were generated by linear interpolation between the optimised geometries of the starting material and the product, and the resolution of the reaction path was increased by interpolating between the structures in the path using a custom script (see ESI). Thermodynamic properties and reaction barrier heights are reported as non standard-state corrected gas phase energies.

**Supporting information**

Selected NMR spectra; details of the line shape analyses; selected calculated thermodynamic, spectroscopic, geometric, and electronic properties of **1**, **1' – 6'**; X-ray crystallographic data for **6** in CIF format; optimized geometries in Cartesian coordinates (.xyz); and a python script for calculating NEB trajectories (.txt). This material is available free of charge via the Internet at http://pubs.acs.org.

**Acknowledgements**

We thank the University of Warwick (R.E.A.), the Australian Research Council (C.A.O; grants DP110105530, DP130100483 and a Queen Elisabeth II fellowship) and the Royal Society (A.B.C.) for financial support. Crystallographic data was collected using a diffractometer purchased through support from Advantage West Midlands and the European Regional Development Fund.

**References**


[1] (a) Dröge, T.; Glorius, F. *Angew. Chem. Int. Ed.* **2010**, *49*, 6940–6952; (b) Hahn, F. E.; Jahnke, M. C. *Angew. Chem. Int. Ed.* **2008**, *47*, 3122–3172.

[2] (a) van Koten, G., Milstein, D. Eds.; *Top. Organomet. Chem.* **2013**, *40*, 1-352; (b) Albrecht, M.; Lindner, M. M. *Dalton Trans.* **2011**, *40*, 8733–8744; (c) van der Boom, M. E.; Milstein, D. *Chem. Rev.* **2003**, *103*, 1759–1792; (d) Albrecht, M.; van Koten, G. *Angew. Chem. Int. Ed.* **2001**, *40*, 3750–3781.

[3] (a) Poyatos, M.; Mata, J. A.; Peris, E. *Chem. Rev.* **2009**, *109*, 3677–3707; (b) Pugh, D.; Danopoulos, A. A. *Coord. Chem. Rev.* **2007**, *251*, 610–641; (c) Peris, E.; Crabtree, R. H. *Coordin. Chem. Rev.* **2004**, *248*, 2239–2246.

[4] Representative examples in catalysis: (a) Filonenko, G. A.; Cosimi, E.; Lefort, L.; Conley, M. P.; Copéret, C.; Lutz, M.; Hensen, E. J. M.; Pidko, E. A. *ACS Catal.* **2014**, *4*, 2667–2671; (b) Chianese, A. R.; Drance, M. J.; Jensen, K. H.; McCollom, S. P.; Yusufova, N.; Shaner, S. E.; Shopov, D. Y.; Tendler, J. A. *Organometallics* **2014**, *33*, 457–464; (c) Knapp, S. M. M.; Shaner, S. E.; Kim, D.; Shopov, D. Y.; Tendler, J. A.; Pudalov, D. M.; Chianese, A. R. *Organometallics* **2014**, *33*, 473–484; (d) Hernández-Juárez, M.; Vaquero, M.; Álvarez, E.; Salazar, V.; Suárez, A. *Dalton Trans.* **2013**, *42*, 351–354; (e) Chianese, A. R.; Shaner, S. E.; Tendler, J. A.; Pudalov, D. M.; Shopov, D. Y.; Kim, D.; Rogers, S. L.; Mo, A. *Organometallics* **2012**, *31*, 7359–7367; (f) Serra, D.; Cao, P.; Cabrera, J.; Padilla, R.; Rominger, F.; Limbach, M. *Organometallics* **2011**, *30*, 1885–1895; (g) Sun, Y.; Koehler, C.; Tan, R.; Annibale, V. T.; Song, D. *Chem. Commun.* **2011**, *47*, 8349–8351; (h) Inamoto, K.; Kuroda, J.-I.; Kwon, E.; Hiroya, K.; Doi, T. *J. Organomet. Chem.* **2009**, *694*, 389–396; (i) Wei, W.; Qin, Y.; Luo, M.; Xia, P.; Wong, M. S. *Organometallics* **2008**, *27*, 2268–2272; (j) Bauer, E. B.; Andavan, G. T. S.; Hollis, T. K.; Rubio, R. J.; Cho, J.; Kuchenbeiser, G. R.; Helgert, T. R.; Letko, C. S.; Tham, F. S. *Org Lett* **2008**, *10*, 1175–1178; (k) Loch, J. A.; Albrecht, M.; Peris, E.; Mata, J.; Faller, J. W.; Crabtree, R. H. *Organometallics* **2002**, *21*, 700–706.

[5] Miecznikowski, J. R.; Gründemann, S.; Albrecht, M.; Mégret, C.; Clot, E.; Faller, J. W.; Eisenstein, O.; Crabtree, R. H. *Dalton Trans.* **2003**, 831–838.

[6] (a) Saito, S.; Azumaya, I.; Watarai, N.; Kawasaki, H.; Yamasaki, R. *Heterocycles* **2009**, *79*, 531–548; (b) Hahn, F. E.; Jahnke, M. C.; Pape, T. *Organometallics* **2007**, *26*, 150–154; (c) Hahn, F. E.; Jahnke, M. C.; Gomez-Benitez, V.; Morales-Morales, D.; Pape, T. *Organometallics* **2005**, *24*, 6458–6463; (d) Gründemann, S.; Albrecht, M.; Loch, J. A.; Faller, J. W.; Crabtree, R. H. *Organometallics* **2001**, *20*, 5485–5488.

[7] Schultz, K. M.; Goldberg, K. I.; Gusev, D. G.; Heinekey, D. M. *Organometallics* **2011**, *30*, 1429–1437.

[8] For an example illustrating a correlation between structural dynamics and enantioselectivitiy in a series of rhodium NHC complexes see: Jeletic, M. S.; Lower, C. E.; Ghiviriga, I.; Veige, A. S. *Organometallics* **2011**, *30*, 6034–6043.

[9] Andrew, R. E.; Chaplin, A. B. *Dalton Trans.* **2014**, *43*, 1413–1423.

[10] (a) Danopoulos, A. A.; Tulloch, A. A. D.; Winston, S.; Eastham, G.; Hursthouse, M. B. *Dalton Trans.* **2003**, 1009–1015; (b) Tulloch, A. A. D.; Danopoulos, A. A.; Tizzard, G. J.; Coles, S. J.; Hursthouse, M. B.; Hay-Motherwell, R. S.; Motherwell, W. B. *Chem. Commun.* **2001**, 1270–1271.

[11] Andrew, R. E.; Chaplin, A. B. *Inorg. Chem.* **2015**, *54*, 312 – 322.

[12] At 298 K and 1 atm partial pressure, the [CO] in $CHCl_3$ and 1,2-$C_2H_4Cl_2$ are 8.5 mM and 6.0 mM, respectively (R. W. Cargill, Ed. *IUPAC Solubility Data Series: Carbon Monoxide*; Pergamon Press: Oxford, **1990**, Vol. 43). The [CO] in $CH_2Cl_2$ under these conditions is presumably of similar magnitude.

[13] As justification for the use of *N*-methyl analogues, we note the highly flexible nature of the dodecamethylene spacer apparent from preceding experimental work using CNC-based pincer complexes [ref. 9,11].

[14] Zhao, Y.; Truhlar, D. G. *Theor. Chem. Acc.* **2008**, *120*, 215-241.

[15] (a) Hehre, W. J.; Ritchfield, R. ; Pople, J. A. *J. Chem. Phys.* **1972**, 2257-2261; (b) Francl, M. M.; Petro, W. J.; Hehre, W. J.; Binkley, J. S.; Gordon, M. S.; DeFrees, D. J.; Pople, J. A. *J. Chem. Phys.* **1982**, 77, 3654-3665.

[16] Implicit solvent models were avoided as these are generally inaccurate for charged species: see for example, Ohlin, C. A.; Rustad, J. R.; Casey, W. H. *Dalton Trans.* **2014**, *43*, 14533-14536.

[17] Mills, G.; Jónsson, H. *Phys. Rev. Lett.* **1994**, 72, 1124-1128.

[18] Although only applicable to isolated ions in the gas phase, the calculated ν(CO) frequencies and intensities for **1'**, **4'** and **5'** are fully consistent with this assignment (see Table S1).

[19] Douvris, C.; Reed, C. A. *Organometallics* **2008**, *27*, 807–810.

[20] Chaplin, A. B. *Organometallics* **2014**, *33*, 3069–3077.

[21] M. Brookhart, M. L. H. Green, G. Parkin, *Proc. Natl. Acad. Sci. USA* **2007**, *104*, 6908–6914.

[22] Buschmann, W. E.; Miller, J. S.; Bowman-James, K.; Miller, C. N. *Inorg. Synth.* **2002**, *33*, 83−91.

[23] McCleverty, J. A.; Wilkinson, G.; Lipson, L. G.; Maddox, M. L.; Kaesz, H. D. *Inorg. Synth.* **1990**, *28*, 84−86.

[24] Valie, M.; Bylaska, E. J.; Govind, N.; Kowalski, K.; Straatsma, T. P.; Van Dam, H. J. J.; Wang, D.; Nieplocha, J.; Apra, E.; Windus, T. L.; De Jong, W. A. *Comput. Phys. Commun.* **2010**, *181*, 1477-1489.

[25] Frisch, M. J.; Trucks, G. W.; Schegel, H. B. *et al.*, *Gaussian 09 Revision D.01*, Gaussian inc., Wallingford CT, 2009.